

Imprecision plateaus in quantum steering

Elna Svegborn,¹ Nicola d'Alessandro,¹ Otfried Gühne,² and Armin Tavakoli¹

¹Physics Department and NanoLund, Lund University, Box 118, 22100 Lund, Sweden.

²Naturwissenschaftlich-Technische Fakultät, Universität Siegen, Walter-Flex-Straße 3, 57068 Siegen, Germany
(Dated: August 23, 2024)

We study tests of quantum steering in which the trusted party does not have perfect control of their measurements. We report on steering inequalities that remain unaffected when introducing up to a threshold magnitude of measurement imprecision. This phenomenon, which we call an imprecision plateau, thus permits a departure from the standard assumption of idealised measurements without any incurring cost to the detection power of steering experiments. We provide an explanation for why imprecision plateaus are possible, a simple criterion for their existence and tools for analysing their properties. We also demonstrate that these plateaus have natural applications when the assumption of perfect measurements is relaxed: they allow for maintaining both the noise- and loss-robustness of standard steering tests and the performance rate of idealised one-sided device-independent random number generators.

Introduction.— Quantum steering is the impossibility of hidden variable theories to explain how quantum measurements on one particle can alter the local state of another particle. The scenario can be understood as a black-box party, Alice, influencing the lab of another party, Bob, in a way that proves shared entanglement. The last many years have seen much interest in studying quantum steering in theory and experiments [1, 2], and developing its applications within e.g. one-sided device-independent quantum key distribution [3, 4], randomness certification [5, 6] and quantum teleportation [7].

In the steering scenario, Alice selects an input, x , and performs a corresponding measurement, $\{A_{a|x}\}_a$, on her share of a bipartite state ρ_{AB} . The (sub-normalised) states created remotely for Bob become $\sigma_{a|x} = \text{tr}_A(A_{a|x} \otimes \mathbb{1} \rho_{AB})$. The set $\{\sigma_{a|x}\}$ is called the steering assemblage. Bob must now determine whether the assemblage can be modelled via a local hidden state (LHS), i.e. whether it admits the form $\sigma_{a|x} = \sum_{\lambda} p(\lambda) p(a|x, \lambda) \sigma_{\lambda}$, where λ is a hidden variable and σ_{λ} is the hidden quantum state [8]. If the answer is negative, the assemblage is steerable, implying that ρ_{AB} is entangled. To detect steerability, Bob must select an input y and perform an associated measurement $\{B_{b|y}^{\text{targ}}\}_b$. The assemblage demonstrates steering if and only if the input/output statistics can violate a suitable inequality that is respected by all local hidden state (LHS) models but not by quantum theory [8]. Such a steering inequality takes the form

$$\mathcal{W}_0 \equiv \sum_{a,b,x,y} c_{abxy} \text{tr}(\sigma_{a|x} B_{b|y}^{\text{targ}}) \stackrel{\text{LHS}}{\leq} \beta_0, \quad (1)$$

where c_{abxy} are arbitrary real coefficients and β_0 is the tight bound for LHS models.

However, standard steering inequalities (1) require a strong assumption: that Bob is able to *perfectly* implement his targeted measurements. This is an idealisation to which experiments can only aspire. A series of works, focused on experiments for tomography [9], communication [10, 11], entanglement [9, 12, 13], and steering [14, 15], have shown that if Bob's operations only nearly correspond to those targeted, it can lead to a high risk of false positives. For example, the perhaps most well-known test of two-qubit steering involves Alice and Bob measuring the three Pauli observables $\{X, Y, Z\}$.

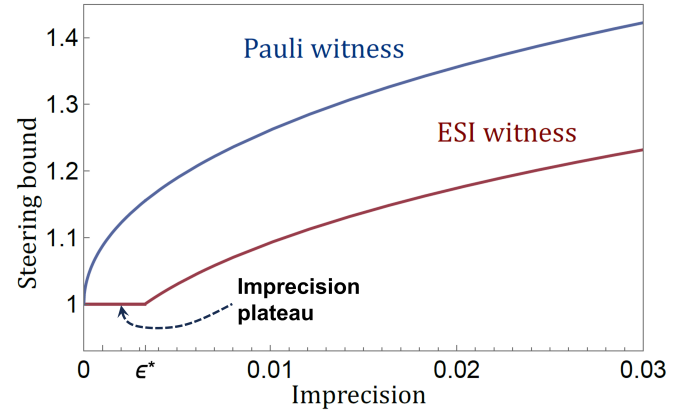


FIG. 1. Imprecise measurements for the trusted party typically leads to stronger LHS correlations, i.e. a higher steering bound (blue curve). However, some steering witnesses remain unchanged, up to a critical value, even though the measurements are increasingly uncontrolled. This leads to an imprecision plateau (red curve).

Specifically, in an LHS model, this “Pauli witness” is

$$\mathcal{W}_0^{\text{pauli}} = \frac{1}{\sqrt{3}} (\langle A_1, X \rangle + \langle A_2, Y \rangle + \langle A_3, Z \rangle) \leq 1 \quad (2)$$

for arbitrary observables with eigenvalues ± 1 of Alice [16, 17], whereas quantum theory achieves $\mathcal{W}_0^{\text{pauli}} = \sqrt{3}$. However, if Bob's lab observables turn out to have only a nearly perfect fidelity of, say, 99.5%, over 25% of the possible quantum violation range can be explained by false positives stemming from LHS models [15]. The high-sensitivity to small measurement imprecisions is illustrated for the Pauli witness by the steep increase around the origin of the blue curve in Fig. 1. Similar effects arise for other common steering inequalities [15], and only some refined methods are known that can detect steering without this drawback [14].

It has been proposed to eliminate the perfect-measurement assumption by replacing it with a quantitative limitation of Bob's lack of control. Refs. [9, 13, 15, 18] consider that Bob aims to perform a target measurement corresponding to a basis $\{|e_b\rangle\}$, but instead implements a different lab measurement

$\{E_b\}$. The lab measurement can be subject to arbitrary imperfection; it is only assumed to be a good approximation of the target measurement, fulfilling the constraint

$$\langle e_b | E_b | e_b \rangle \geq 1 - \epsilon_b, \quad (3)$$

for some small imprecision parameter $\epsilon_b \in [0, 1]$. This definition has the advantages of being platform-independent and operationally meaningful. Indeed, ϵ_b can be estimated with small resources in the lab. However, when permitting imprecise measurements in our model, we reduce our assumed prior knowledge of the experiment. This means that the LHS bound in (1) in general must increase to account for all measurements compatible with the condition (3), leading to an ϵ -dependent criterion, $\mathcal{W}_\epsilon \leq \beta_\epsilon$ (e.g., the blue curve in Fig. 1).

Here, we reveal that it is possible to conduct steering tests without assuming idealised measurements that nevertheless cost no additional detection power. Specifically, we show that there exists steering inequalities of the form (1) where the LHS bound does not change when relaxing the assumption of perfectly controlled measurements up to a critical imprecision magnitude ϵ^* . That is, when the imprecision is below the threshold, i.e. $\epsilon \leq \epsilon^*$, the steering inequality remains $\mathcal{W}_\epsilon \leq \beta_0$. This corresponds to an *imprecision plateau* for steering inequalities, in which the ability to detect steering remains as good as if the measurements had been assumed perfect. This phenomenon is illustrated by the red curve in Fig. 1. We give an intuitive explanation for the existence of imprecision plateaus in terms of properties of well-chosen steering witnesses. This also provides a simple way to identify witnesses that support a plateau. For our key example, we analytically characterise the plateau's length (see ϵ^* in Fig. 1), while for generic steering witnesses we develop both analytical and numerical relaxation methods to estimate it. We then proceed to showcase the utility of these plateaus in tests of steering and its quantum information applications.

Imprecision plateaus.— To prove the existence of and to understand imprecision plateaus, we consider a steering witness based on the so-called Elegant Bell Inequality [19, 20], which we, in analogy, will refer to as the Elegant Steering Inequality (ESI). In the ESI scenario, Alice and Bob have four and three inputs, respectively, and binary outputs. Alice's measurements are unknown whereas Bob's three target measurements correspond to the Paulis, i.e., $B_1^{\text{targ}} = X$, $B_2^{\text{targ}} = Y$, and $B_3^{\text{targ}} = Z$. For binary measurements $\{O_0, O_1\}$, we define observables as $O = O_0 - O_1$. The ESI reads

$$\begin{aligned} \mathcal{W}_0^{\text{ESI}} = & \frac{1}{4} \left(\langle (A_1 + A_2 - A_3 - A_4) \otimes B_1^{\text{targ}} \rangle \right. \\ & + \langle (A_1 - A_2 + A_3 - A_4) \otimes B_2^{\text{targ}} \rangle \\ & \left. + \langle (A_1 - A_2 - A_3 + A_4) \otimes B_3^{\text{targ}} \rangle \right) \stackrel{\text{LHS}}{\leq} 1, \quad (4) \end{aligned}$$

which can be computed as a largest-eigenvalue problem.

If the parties share the maximally entangled state $|\phi^+\rangle = (|00\rangle + |11\rangle)/\sqrt{2}$ and Alice's measurements form a regular tetrahedron on the Bloch sphere, one achieves the maximal violation $\mathcal{W}_0 = \sqrt{3}$ and the expression (4) reduces to the Pauli witness (2) with optimal choices of observables. Many states

that do not violate any Bell inequality violate the ESI: the standard example is the isotropic state $\rho_v = v |\phi^+\rangle\langle\phi^+| + (1-v) \frac{\mathbb{1}}{4}$ which is Bell-local for $v \lesssim 0.6875$ [21] but violates the ESI if $v > \frac{1}{\sqrt{3}} \approx 0.577$.

Now, we replace the target measurements in (4) with ϵ -imprecise measurements, $\{B_y^\epsilon\}$, and set out to compute the new, ϵ -dependent, LHS bound. From Eq. (3), one finds that this means considering all qubit observables such that $\text{tr}(B_y^{\text{targ}} B_y^\epsilon) \geq 2 - 4\epsilon$. Since the witness is linear, we need only to consider all deterministic input-output strategies of Alice. Labelling them by $(a_1, a_2, a_3, a_4) \in \{0, 1\}^4$, the values of \mathcal{W}_ϵ become [22]

$$\begin{aligned} \text{C1} \quad & (0, 0, 0, 0) \Rightarrow \mathcal{W}_\epsilon = 0 \\ \text{C2} \quad & \begin{cases} (0, 0, 0, 1) \Rightarrow \mathcal{W}_\epsilon = 2\langle B_1^\epsilon + B_2^\epsilon - B_3^\epsilon \rangle_\psi \\ (0, 0, 1, 0) \Rightarrow \mathcal{W}_\epsilon = 2\langle B_1^\epsilon - B_2^\epsilon + B_3^\epsilon \rangle_\psi \\ (1, 0, 1, 1) \Rightarrow \mathcal{W}_\epsilon = 2\langle B_1^\epsilon - B_2^\epsilon - B_3^\epsilon \rangle_\psi \\ (0, 1, 1, 1) \Rightarrow \mathcal{W}_\epsilon = 2\langle B_1^\epsilon + B_2^\epsilon + B_3^\epsilon \rangle_\psi \end{cases} = f^*(\epsilon) \\ \text{C3} \quad & \begin{cases} (0, 0, 1, 1) \Rightarrow \mathcal{W}_\epsilon = 4\langle B_1^\epsilon \rangle_\psi \\ (0, 1, 0, 1) \Rightarrow \mathcal{W}_\epsilon = 4\langle B_2^\epsilon \rangle_\psi \\ (0, 1, 1, 0) \Rightarrow \mathcal{W}_\epsilon = 4\langle B_3^\epsilon \rangle_\psi \end{cases} = g^*(\epsilon). \end{aligned} \quad (5)$$

Due to the Bloch sphere symmetry and the unbiasedness of the three target measurements, we see that these eight cases reduce to just three qualitatively different classes, as indicated above. Class 1 is trivial. For class 2, the steering bound is $f(\epsilon) \equiv \max f^*(\epsilon) = \frac{\sqrt{3}}{2} (1 + 2\sqrt{2\epsilon(1-\epsilon)} - 2\epsilon)$, which is proven in Appendix A. Note that for $\epsilon = 0$ we have $f = \frac{\sqrt{3}}{2}$. Next, we make the key observation: the value for class 3 is *independent* of ϵ , because trivially $g(\epsilon) \equiv \max g^*(\epsilon) = 1$. Since $g(0) > f(0)$, this is the LHS bound appearing in (4). Crucially, the bound $\mathcal{W}_\epsilon^{\text{ESI}} \leq 1$ remains valid until ϵ is large enough for $f(\epsilon)$ to overtake $g(\epsilon) = 1$. This happens at

$$\epsilon^* = \frac{1}{2} - \frac{1}{3\sqrt{3}} - \frac{1}{3}\sqrt{\frac{5}{6}} \approx 3.3 \times 10^{-3}. \quad (6)$$

Thus, the ESI witness under imprecise measurements becomes $\mathcal{W}_\epsilon^{\text{ESI}} \leq 1$ for $\epsilon \leq \epsilon^*$ and $\mathcal{W}_\epsilon^{\text{ESI}} \leq f(\epsilon)$ for $\epsilon^* < \epsilon \leq (3 - \sqrt{3})/6$, where the upper demarcation corresponds to the maximal value of f [23]. This threshold implies the imprecision plateau (see red curve in Fig. 1) and ϵ^* can therefore be interpreted as the plateau's length.

We can now identify the characteristic property of generic steering witnesses which support an imprecision plateau. For standard steering ($\epsilon = 0$), all deterministic strategies associated with the tight steering bound must correspond to witness expressions [as in Eq. (5)] that depend only on a *single* input of Bob. In a LHS model, this permits Bob's local state to exactly align itself with the relevant observable independently of ϵ . This is impossible when more than a single observable is relevant in the expression, because the metric distance of two observables will be ϵ -dependent. This observation reduces the question of whether an arbitrary steering witness

supports an imprecision plateau to what is essentially a set of largest-eigenvalue problems.

It is important to note that the imprecision plateau as a phenomenon is *independent* of the specific quantifier used to describe the loss of control over Bob's measurements. For instance, we have assumed the dimension of the lab measurement in order to make possible the fidelity-interpretation of Eq. (3). For instance, following [24], we can instead adopt dimension-agnostic quantifier, e.g. a limitation on the norm of the anti-commutators of the lab observables $\|\{B_y, B_{y'}\}\|_\infty \leq \epsilon$. We still have $g(\epsilon) = 1$ for class 3 and via the Cauchy-Schwarz inequality we obtain for class 2, $f^*(\epsilon) \leq 2\sqrt{3 + \sum_{j < k} \langle \{B_j^\epsilon, B_k^\epsilon\} \rangle_\psi} \leq 2\sqrt{3(1 + \epsilon)} = f(\epsilon)$. For $\epsilon \leq \frac{1}{3}$, $f(\epsilon)$ does not exceed $g(\epsilon) = 1$ and hence, we have a plateau in ϵ .

Semidefinite programming methods.— While the ESI is simple enough for analytically determining the plateau's length, this is in general rarely the case. Consider that we are given an arbitrary steering witness and we find that it supports a plateau. How can we bound the plateau's length? Already for the more experimentally relevant variant of the ESI, in which each of Bob's three measurements has a different imprecision parameter, $\vec{\epsilon} = (\epsilon_X, \epsilon_Y, \epsilon_Z)$, we have been unable to solve the problem exactly. One possibility is to apply the main theorem of Ref. [15] to each of the deterministic strategies of Alice. This theorem gives a bound on the operators in terms of the imprecision parameter and allows one to compute ϵ -dependent upper bounds on any steering witness \mathcal{W}_ϵ as perturbations to the standard steering inequality (1), but it does not give a tight bound (see Appendix B). Another, less rigorous option, also discussed in Appendix B, is to use a Taylor approximation in the relevant regime of small imprecision. This gives better bounds, but still not tight. Instead, the we address the problem of bounding the plateau length using semidefinite programming (SDP) relaxations based on moment matrices [25].

The method, discussed in detail in Appendix C, is based on three main ideas. Firstly, contrasting the common approach to Bell-type scenarios [26, 27], we define a tracial moment matrix, $\Gamma_{u,v} = \text{tr}(u^\dagger v)$, where u and v are monomials of observables in the selected relaxation. Secondly, we use the idea of [28] to add dimensionality constraints on Γ by constructing a basis of moment matrices via random sampling. Thirdly, we follow the idea of [10] and explicitly insert the target measurements into the monomial set to incorporate the fidelity constraints into the SDP relaxation. Combined, this lets us express the steering witness as a linear combination over Γ and realise (3) as linear constraints. Given that Γ is positive semidefinite by construction, it can be solved as an SDP. To showcase the usefulness of this method, we have applied it to the ESI witness with the three independent imprecision parameters. Already at first level relaxation, corresponding to an SDP matrix of dimension 14 with 19 variables, it systematically returns bounds on the plateau length that match our brute-force numerical search values up to at worst five decimals. The plateau length in ϵ_Z as a function of ϵ_X and ϵ_Y is given in Appendix C.

Application to noise and loss.— Imprecision plateaus have natural applications in experiments that recognise the lack of perfect measurement control. Typically, as we have exemplified in Fig. 1 for the Pauli witness (2), the quantum violation gap rapidly shrinks when accounting for imperfect measurements. This is equivalent to the decrease of the corresponding noise tolerance of steering. However, the plateau permits experiments to account for measurement imperfections while maintaining the noise-tolerance associated with idealised measurements. For example, for perfect measurements ($\epsilon = 0$), both the Pauli witness and the ESI witness detect steering for the isotropic state ρ_v when $v > \frac{1}{\sqrt{3}} \approx 0.577$. However, when permitting measurement imprecision corresponding to the plateau length ϵ^* , the equivalence is far gone. The former now requires $v \gtrsim 0.667$ whereas the latter still has $v \gtrsim 0.577$. Note that a nonlinear test for steering exists, where Bob implements Pauli measurements on qubits without any assumption on the precision [14]. This works for any $v \gtrsim 0.577$ too, but is not straightforward to generalize to arbitrary systems.

A similar advantage applies for scenarios with detection losses, i.e., when Alice's measurement fails with probability $\eta \in [0, 1]$. Since in our picture the measurement errors of Bob are uncontrolled, we do not allow him to actively use the ϵ -cone around his target measurement toward closing the detection loophole. Instead, we assume that he performs the target measurements. It is well-known that the critical efficiency, η_{crit} , needed for demonstrating steering is much lower than the efficiency needed for a Bell inequality violation, where Bob's measurements are entirely uncharacterised [29, 30]. Therefore, with the gradual loss of measurement control, one expects η_{crit} to increase towards the Bell inequality limit. However, the imprecision plateau permits us to circumvent this problem for imprecision magnitudes within the plateau. For perfect measurement control, the critical detection efficiency for both the Pauli witness and the ESI witness is $\eta_{\text{crit}} = \frac{1}{3}$. However, at imprecision $\epsilon = \epsilon^*$, the advantage becomes large: the ESI witness still has $\eta_{\text{crit}} = \frac{1}{3}$ whereas the Pauli witness now requires $\eta_{\text{crit}} \approx 0.606$. In Appendix D, we compute the optimal witness values at fixed detection efficiency.

Application: random number generation.— Imprecision plateaus also enable advantages in one-sided device-independent protocols. We showcase this for quantum random number generation. Using the ESI witness as a tested, we show that for imprecisions within the plateau, one can both certify randomness whenever the original steering inequality is violated and obtain the same rate of randomness as when assuming perfect measurements. Thus, the performance of the protocol is fully maintained while eliminating idealisations that otherwise may be used to compromise the security.

We certify randomness from Alice's output averaged over her four possible inputs. The randomness is given by $R = -\log_2(P_g)$ where $P_g = \max \frac{1}{4} \sum_{a,x} p(a|x)$ is the average probability of an eavesdropper guessing her outcome [31], maximised over all strategies. Thus, we must compute the largest possible P_g compatible with the observed value of the ESI witness. This can be achieved by evaluating P_g separately for each of Alice's deterministic strategies. When $\epsilon = 0$, each

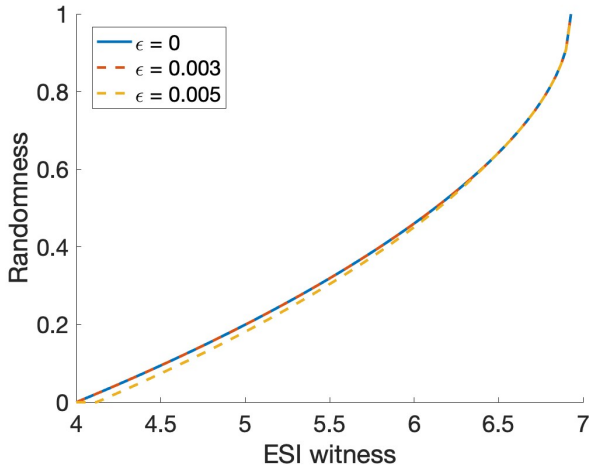


FIG. 2. The performance of the randomness generation remains unchanged when introducing measurement imprecisions below the plateau length (blue and red curve). However, imprecisions above the plateau length lead to the expected decrease in noise tolerance and generation rate (yellow curve).

of these optimisations can be straightforwardly cast as an SDP. When $\epsilon > 0$, we can bound P_g from above (corresponding to a lower bound on R) by using the previously discussed SDP relaxation method. This is applied separately to each of the deterministic strategies [32]. To this end, we have selected $\epsilon = 3 \times 10^{-3} < \epsilon^*$ and employed a moment matrix of size 296 featuring 1371 variables. The randomness rates are illustrated in Fig. 2. Our certified randomness bound is essentially equal to the amount of randomness obtained for $\epsilon = 0$, with a worst-case difference of $\Delta R = 0.0016$. The small discrepancy is likely due to our choice of relaxation level; which is a compromise between accuracy and practicality. This illustrates the maintained protocol performance in face of measurement imprecisions. In contrast, when operating outside the plateau, e.g. at $\epsilon = 5 \times 10^{-5} > \epsilon^*$, we cannot maintain neither the randomness rate nor the noise tolerance. This is illustrated by the yellow curve in Fig. 2, which is an upper bound on R obtained from numerical search. It implies a clear reduction in the performance when not having access to the imprecision plateau.

Beyond qubits and rank-one measurements.— Higher-dimensional measurements are often harder to control than qubit measurements. This makes it relevant to consider imprecision plateaus also beyond qubit systems. In a line of reasoning similar to the ESI example, we have drawn inspiration from a family of Bell inequalities [33] in order to construct a steering inequality supporting an imprecision plateau for four-dimensional systems. This inequality is maximally violated using maximally entangled states and target measurements corresponding to tensor products of specific Pauli observables. The steering inequality and the analysis of its imprecision plateau is given in Appendix E. Importantly, since the analysis is based on high-dimensional systems, we cannot determine the plateau length by using the Bloch sphere. Instead, we have been able to solve this problem exactly by using a

more general analytical procedure. In Appendix F, we prove a natural generalisation of the main theorem in Ref. [15]. The theorem of [15] requires the target measurements to be rank-one projections. However, in our generalisation, the projective target measurements are permitted to have arbitrary rank. This is often useful, for instance when considering products of Pauli observables as target measurements.

Discussion.— Quantum steering experiments are commonly performed under the assumption that the trusted party has perfectly controlled measurements. This is an unrealistic assumption, whose near-validity is also rarely evidenced in practice. For steering scenarios, the problem of how to make witness tests valid under arbitrary imprecision was addressed in Ref. [15]. However, the main drawback is that most of the well-known steering witnesses rapidly lose their detection power even as tiny imprecision is introduced. In this work, we have shown a sharp contrast to this observation, namely that well-chosen tests of steering can remain unchanged even when perfect control of the trusted measurement is relaxed. We have seen how this is made possible in steering because of the phenomenon of imprecision plateaus. These plateaus lead to several natural questions. How does one construct steering witnesses that both have a long imprecision plateau and detect entanglement that is far from Bell nonlocal? Furthermore, given the relevance of high-dimensional systems for steering, how can one find witnesses supporting a long a relevant plateau for systems of arbitrary dimension? It seems likely that imprecision plateaus also should appear more broadly, for example in multipartite steering or steering with quantum inputs [34, 35]. It is natural to ask if imprecision plateaus also are possible in other quantum correlation scenarios, e.g., for entanglement witnesses.

We have also shown that imprecision plateaus have natural applications. These can be divided into two types. Firstly, the plateaus pave the way for tests of steering that remove the undesirable assumption of perfect measurements, thus becoming more resilient to false positives, but without any cost to neither the noise or loss requirements of the experiment. We have exemplified these advantages in our analysis of the ESI. Importantly, the plateau lengths that we have found are significantly larger than the imprecision parameters reported in a recent experiment [18]. Secondly, they can be used to make one-sided device-independent quantum information protocols more faithful while maintaining the performance of the original, idealised, protocol. We illustrated this possibility in a proof-of-principle analysis of a quantum random number generator. This suggests that similar advantages may be more widely possible.

ACKNOWLEDGMENTS

We thank Alexander Bernal, Elisa Monchetti and Carles Roch i Carceller for discussions. This work is supported by the Wenner-Gren Foundation, by the Knut and Alice Wallenberg Foundation through the Wallenberg Center for Quantum Technology (WACQT), by the EDU-WACQT program funded by Marianne and Marcus Wallenberg Foundation, by

the Swedish Research Council under Contract No. 2023-03498, by the Deutsche Forschungsgemeinschaft (DFG, German Research Foundation, project numbers 447948357 and 440958198, by the Sino-German Center for Research Pro-

motion (Project M-0294), and the German Ministry of Education and Research (Project QuKuK, BMBF Grant No. 16KIS1618K).

-
- [1] R. Uola, A. C. S. Costa, H. C. Nguyen, and O. Gühne, Quantum steering, *Reviews of Modern Physics* **92**, 015001 (2020).
- [2] D. Cavalcanti and P. Skrzypczyk, Quantum steering: a review with focus on semidefinite programming, *Reports on Progress in Physics* **80**, 024001 (2016).
- [3] C. Branciard, E. G. Cavalcanti, S. P. Walborn, V. Scarani, and H. M. Wiseman, One-sided device-independent quantum key distribution: Security, feasibility, and the connection with steering, *Phys. Rev. A* **85**, 010301 (2012).
- [4] X. Ma and N. Lütkenhaus, Improved data post-processing in quantum key distribution and application to loss thresholds in device independent QKD, *Quantum Information and Computation* **12**, 0203 (2011), [arXiv:1109.1203 \[quant-ph\]](https://arxiv.org/abs/1109.1203).
- [5] Y. Z. Law, L. P. Thinh, J.-D. Bancal, and V. Scarani, Quantum randomness extraction for various levels of characterization of the devices, *Journal of Physics A: Mathematical and Theoretical* **47**, 424028 (2014).
- [6] Y. Li, Y. Xiang, X.-D. Yu, H. C. Nguyen, O. Gühne, and Q. He, Randomness certification from multipartite quantum steering for arbitrary dimensional systems, *Physical Review Letters* **132**, 080201 (2024).
- [7] Q. He, L. Rosales-Zárate, G. Adesso, and M. D. Reid, Secure continuous variable teleportation and Einstein-Podolsky-Rosen steering, *Physical Review Letters* **115**, 180502 (2015).
- [8] H. M. Wiseman, S. J. Jones, and A. C. Doherty, Steering, entanglement, nonlocality, and the Einstein-Podolsky-Rosen paradox, *Physical Review Letters* **98**, 140402 (2007).
- [9] D. Rosset, R. Ferretti-Schöbitz, J.-D. Bancal, N. Gisin, and Y.-C. Liang, Imperfect measurement settings: Implications for quantum state tomography and entanglement witnesses, *Physical Review A* **86**, 062325 (2012).
- [10] A. Tavakoli, Semi-device-independent framework based on restricted distrust in prepare-and-measure experiments, *Physical Review Letters* **126**, 210503 (2021).
- [11] J. Pauwels, S. Pironio, E. Woodhead, and A. Tavakoli, Almost qudits in the prepare-and-measure scenario, *Physical Review Letters* **129**, 250504 (2022).
- [12] T. Moroder and O. Gittsovich, Calibration-robust entanglement detection beyond Bell inequalities, *Phys. Rev. A* **85**, 032301 (2012).
- [13] S. Morelli, H. Yamasaki, M. Huber, and A. Tavakoli, Entanglement detection with imprecise measurements, *Physical Review Letters* **128**, 250501 (2022).
- [14] T. Moroder, O. Gittsovich, M. Huber, R. Uola, and O. Gühne, Steering maps and their application to dimension-bounded steering, *Physical Review Letters* **116**, 090403 (2016).
- [15] A. Tavakoli, Quantum steering with imprecise measurements, *Physical Review Letters* **132**, 070204 (2024).
- [16] E. G. Cavalcanti, S. J. Jones, H. M. Wiseman, and M. D. Reid, Experimental criteria for steering and the Einstein-Podolsky-Rosen paradox, *Physical Review A* **80**, 032112 (2009).
- [17] D. J. Saunders, S. J. Jones, H. M. Wiseman, and G. J. Pryde, Experimental EPR-steering using Bell-local states, *Nature Physics* **6**, 845 (2010).
- [18] H. Cao, S. Morelli, L. A. Rozema, C. Zhang, A. Tavakoli, and P. Walther, Genuine multipartite entanglement without fully controllable measurements (2023), [arXiv:2310.11946 \[quant-ph\]](https://arxiv.org/abs/2310.11946).
- [19] N. Gisin, Bell inequalities: Many questions, a few answers, in *Quantum Reality, Relativistic Causality, and Closing the Epistemic Circle: Essays in Honour of Abner Shimony* (Springer Netherlands, Dordrecht, 2009) pp. 125–138.
- [20] A. Tavakoli and N. Gisin, The Platonic solids and fundamental tests of quantum mechanics, *Quantum* **4**, 293 (2020).
- [21] S. Designolle, G. Iommazzo, M. Besançon, S. Knebel, P. Gelß, and S. Pokutta, Improved local models and new Bell inequalities via Frank-Wolfe algorithms, *Physical Review Research* **5**, 043059 (2023).
- [22] We need only to consider eight of Alice’s 16 deterministic strategies because those equivalent under a bit-flip correspond to an irrelevant global minus sign. (.)
- [23] The maximal value is $f = 3/2$ and corresponds to the local hidden variable bound for the witness, i.e. the Elegant Bell Inequality. (.)
- [24] C. de Gois, K. Hansenne, and O. Gühne, Uncertainty relations from graph theory, *Physical Review A* **107**, 062211 (2023).
- [25] A. Tavakoli, A. Pozas-Kerstjens, P. Brown, and M. Araújo, Semidefinite programming relaxations for quantum correlations (2024), [arXiv:2307.02551 \[quant-ph\]](https://arxiv.org/abs/2307.02551).
- [26] M. Navascués, S. Pironio, and A. Acín, Bounding the set of quantum correlations, *Physical Review Letters* **98**, 010401 (2007).
- [27] M. F. Pusey, Negativity and steering: A stronger Peres conjecture, *Physical Review A* **88**, 032313 (2013).
- [28] M. Navascués and T. Vértesi, Bounding the set of finite dimensional quantum correlations, *Physical Review Letters* **115**, 020501 (2015).
- [29] A. J. Bennet, D. A. Evans, D. J. Saunders, C. Branciard, E. G. Cavalcanti, H. M. Wiseman, and G. J. Pryde, Arbitrarily loss-tolerant Einstein-Podolsky-Rosen steering allowing a demonstration over 1 km of optical fiber with no detection loophole, *Physical Review X* **2**, 031003 (2012).
- [30] B. Wittmann, S. Ramelow, F. Steinlechner, N. K. Langford, N. Brunner, H. M. Wiseman, R. Ursin, and A. Zeilinger, Loophole-free Einstein-Podolsky-Rosen experiment via quantum steering, *New Journal of Physics* **14**, 053030 (2012).
- [31] S. Pironio, A. Acín, S. Massar, A. B. de la Giroday, D. N. Matsukevich, P. Maunz, S. Olmschenk, D. Hayes, L. Luo, T. A. Manning, and C. Monroe, Random numbers certified by Bell’s theorem, *Nature* **464**, 1021 (2010).
- [32] P. Mironowicz, A. Tavakoli, A. Hameedi, B. Marques, M. Pawłowski, and M. Bourennane, Increased certification of semi-device independent random numbers using many inputs and more post-processing, *New Journal of Physics* **18**, 065004 (2016).
- [33] A. Tavakoli, B. Marques, M. Pawłowski, and M. Bourennane, Spatial versus sequential correlations for random access coding, *Physical Review A* **93**, 032336 (2016).
- [34] Y.-Y. Zhao, H.-Y. Ku, S.-L. Chen, H.-B. Chen, F. Nori, G.-Y. Xiang, C.-F. Li, G.-C. Guo, and Y.-N. Chen, Ex-

perimental demonstration of measurement-device-independent measure of quantum steering, *npj Quantum Information* **6**, 10.1038/s41534-020-00307-9 (2020).

- [35] S. Kocsis, M. J. W. Hall, A. J. Bennet, D. J. Saunders, and G. J. Pryde, Experimental measurement-device-independent verification of quantum steering, *Nature Communications* **6**, 10.1038/ncomms6886 (2015).
- [36] G. Vallone, Einstein-Podolsky-Rosen steering: Closing the detection loophole with non-maximally-entangled states and arbitrary low efficiency, *Physical Review A* **87**, 020101 (2013).

Appendix A: Proof of the imprecision plateau of the ESI witness

We compute the witness value associated Alice's deterministic strategies, in the main text labelled as class 2, namely

$$f(\epsilon) \equiv \max_{\psi, B_y^\epsilon} f^*(\epsilon) = \max_{\psi, B_y^\epsilon} \frac{1}{2} \langle B_1^\epsilon + B_2^\epsilon + B_3^\epsilon \rangle_\psi. \quad (\text{A1})$$

This entails an optimisation over all states ψ and qubit observables B_y^ϵ , such that they are at least $\epsilon_y = \epsilon$ close to their associated target measurement $B_1^{\text{targ}} = X$, $B_2^{\text{targ}} = Y$, and $B_3^{\text{targ}} = Z$. To get an intuition for how such optimization can be approached, we first give a geometrical argument for how to derive $f(\epsilon)$ and then give a more rigorous proof using the theorem in Ref. [15].

1. Bloch sphere argument

To give an intuition for how to derive $f(\epsilon)$, we start by translating the optimization problem in Eq. (A1) to the Bloch sphere, see schematic illustration in Fig. 3. For perfectly controlled measurements, we find that $\max_{\psi} f^*(\epsilon = 0)$ reaches its maximum value $\sqrt{3}/2$ when ψ is pure and overlaps equally with each of the three orthogonal observables, i.e., when its Bloch vector is given by $\vec{\psi} = (1, 1, 1)/\sqrt{3}$. This is obtained as an eigenvalue problem. In fact, because of the spherical symmetry of the Bloch sphere and the unbiasedness of B_y^ϵ , we find that the maximal value of $f(\epsilon > 0)$ is obtained when ψ remains in the middle of the sphere octant and B_y^ϵ move symmetrically towards it. Consequently, we can w.l.g. express the upper bound of $f(\epsilon)$ in terms of only a single observable, say B_3^ϵ ,

$$f(\epsilon) = \max_{B_y^\epsilon} \frac{1}{2} \langle B_1^\epsilon + B_2^\epsilon + B_3^\epsilon \rangle_\psi = \frac{3}{2} \max_{B_3^\epsilon} \langle B_3^\epsilon \rangle_\psi. \quad (\text{A2})$$

Next, by associating B_3^ϵ with the Bloch vector $\vec{b} = (\sin \theta \cos \varphi, \sin \theta \sin \varphi, \cos \theta)$, where $\theta \in [0, \pi]$, $\varphi \in [0, 2\pi)$, we obtain that

$$\frac{3}{2} \max_{B_3^\epsilon} \langle B_3^\epsilon \rangle_\psi = \max_{B_3^\epsilon} \frac{\sqrt{3}}{2} \vec{b} \times (1, 1, 1). \quad (\text{A3})$$

From the argument that the observables move symmetrically towards ψ , it is clear that the azimuthal angle of \vec{b} can be set to $\varphi = \pi/4$. In addition, from the fidelity constraint

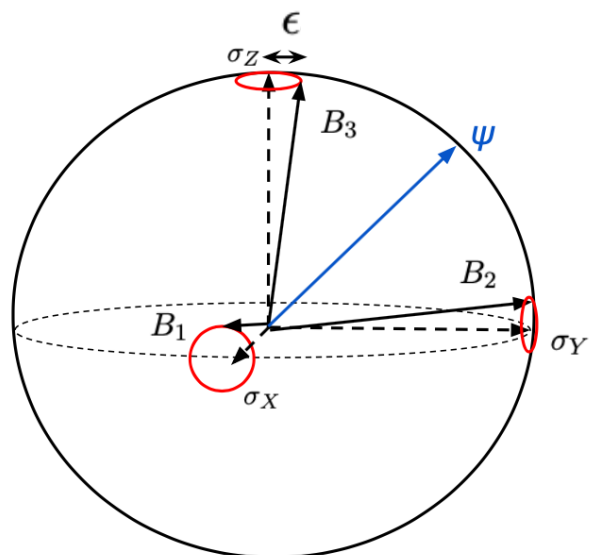


FIG. 3. The imprecise measurements B_y on the Bloch sphere can move in ϵ -cones around the target measurements. We want the total overlap between ψ and B_y to be maximised.

$\text{tr}(B_y^{\text{targ}} B_y^\epsilon) \geq 2 - 4\epsilon$, we get that the polar angle θ fulfills the inequality constraint $\frac{1}{2}(1 + \cos \theta) \geq 1 - \epsilon$. In particular, the optimal choice of θ corresponds to the case of equality. As a result, the $f(\epsilon)$ is maximised when B_3^ϵ 's Bloch vector is

$$\vec{b} = (\sqrt{2}\sqrt{\epsilon(1-\epsilon)}, \sqrt{2}\sqrt{\epsilon(1-\epsilon)}, 1-2\epsilon), \quad (\text{A4})$$

which inserted into (A3) yields

$$f(\epsilon) = \frac{\sqrt{3}}{2} (1 + 2\sqrt{2\epsilon(1-\epsilon)} - 2\epsilon) \quad (\text{A5})$$

We observe that $f(\epsilon)$ increases monotonically from $\sqrt{3}/2$ to $3/2$ as a function of ϵ , where the upper bound corresponds to the local hidden variable bound for the witness. Specifically, from Eq. (A5) we find that the critical magnitude of imprecision at which $f(\epsilon)$ overtakes the standard LHS bound $\beta_0 = 1$ is given by

$$\epsilon^* = \frac{9 - 2\sqrt{3} - \sqrt{30}}{18} \approx 0.00326. \quad (\text{A6})$$

That is, $\beta_0 = 1$ corresponds to the largest value of the LHS bound until we reach an imprecision $\epsilon^* \approx 0.00326$. Thus, we interpret ϵ^* as the length of the imprecision plateau.

2. Proof via theorem of Ref. [15]

We will now show an alternative derivation of the upper bound of (A1) via the theorem of Ref. [15]. Important to note, in Ref. [15] the method derived was applied directly to the witness. Here we apply it to the specific deterministic strategies of the witness.

The theorem states that for any imprecise measurement $B_{b|y}$ at least ϵ_{by} -close in fidelity to the rank-one target measurement $B_{b|y}^{\text{targ}}$ it holds that

$$B_{b|y} \preceq (1 + \mu_{by}) B_{b|y}^{\text{targ}} + \frac{1}{2} \left(\sqrt{\mu_{by}^2 + 4\epsilon_{by}(1 + \mu_{by})} - \mu_{by} \right) \mathbb{1} \quad (\text{A7})$$

where ϵ_{by} is the imprecision parameter associated with the y 'th measurement of Bob with outcome b and the parameter $\mu_{by} \geq -1$ [15]. Since Bob's imprecision parameters are assumed to be equal, i.e., $\epsilon_{by} = \epsilon$, this implies that $\mu_{by} = \mu$. Now, applying Eq. (A7) to $\max_{\psi, B_y^\epsilon} f^*(\epsilon)$, we find that

$$f^*(\epsilon) \leq \min_{\mu \geq -1} \frac{\sqrt{3}}{2} (1 + \mu) + \frac{3}{2} \sqrt{\mu^2 + 4\epsilon(1 + \mu)} = \tilde{f}(\epsilon) \quad (\text{A8})$$

where the state optimally is as $\psi = (\mathbb{1} + (1, 1, 1)/\sqrt{3} \times \vec{\sigma})/2..$

Next, we solve $\frac{\partial \tilde{f}(\epsilon)}{\partial \mu} = 0$ to find the minimum. Of the two possible solutions, we observe that the one corresponding to the smaller value of $\tilde{f}(\epsilon)$ is

$$\mu_{\text{opt}} = -2\epsilon - \sqrt{2}\sqrt{\epsilon(1 - \epsilon)}. \quad (\text{A9})$$

Evaluating $\tilde{f}(\epsilon)$ at $\mu = \mu_{\text{opt}}$ yields

$$f(\epsilon) \leq \frac{\sqrt{3}}{2} \left(1 + 2\sqrt{2\epsilon(1 - \epsilon)} - 2\epsilon \right), \quad (\text{A10})$$

and we thereby recover the result in Eq. (A5). In this case, we find that the theorem of Ref. [15] provides a tight upper bound of the increasing LHS value.

Appendix B: Approximating the plateau length of the ESI witness for $\vec{\epsilon} = (\epsilon_X, \epsilon_Y, \epsilon_Z)$

Consider the ESI scenario in which each of Bob's three measurements is associated with an independent imprecision parameter, such that $\vec{\epsilon} = (\epsilon_X, \epsilon_Y, \epsilon_Z)$. By optimizing $f(\vec{\epsilon}) = \max_{\psi, B_y^{\epsilon_y}} f^*(\vec{\epsilon})$ we can now derive a plateau region by solving $f(\vec{\epsilon}) = 1$ for one of the imprecision parameters, say ϵ_Z , in terms of the other two ϵ_X, ϵ_Y . Although we cannot find an exact analytical solution of this problem we can still approximate it using other methods. We discuss two of them below, but neither is exact.

1. Approximation via theorem of Ref. [15]

To calculate an upper bound of the value of $f(\vec{\epsilon})$ we start by using the theorem from Ref. [15]. Following the same procedure as in Appendix A, applying (A7) to each of Bob's observables in $f^*(\vec{\epsilon})$, with $\epsilon_{by} = \epsilon_y$, yields

$$f^*(\vec{\epsilon}) \leq \max_{\psi} \min_{\mu_i \geq -1} \frac{1}{2} \left\langle \sum_{i=1}^3 (1 + \mu_i) B_i^{\text{targ}} \right\rangle_{\psi} + \frac{1}{2} \sum_{i=1}^3 \sqrt{\mu_i^2 + 4\epsilon_i(1 + \mu_i)}. \quad (\text{B1})$$

Then, the optimal state ψ is the one that aligns with $\sum_{i=1}^3 (1 + \mu_i) B_i^{\text{targ}} = (1 + \mu_1, 1 + \mu_2, 1 + \mu_3) \times \vec{\sigma}$. This gives that

$$f^*(\vec{\epsilon}) \leq \min_{\mu_i \geq -1} \frac{1}{2} \sqrt{\sum_{i=1}^3 (1 + \mu_i)^2} + \frac{1}{2} \sum_{i=1}^3 \sqrt{\mu_i^2 + 4\epsilon_i(1 + \mu_i)} = \tilde{f}(\vec{\epsilon}). \quad (\text{B2})$$

At this point it is challenging to analytically constrain the upper bound further. Thus, to compute the plateau region by solving $\tilde{f}(\vec{\epsilon}) = 1$, we numerically optimize (B2) over μ_i . That is, for fixed values of (ϵ_X, ϵ_Y) , we can find the length of the imprecision plateau in terms of ϵ_Z by successively increasing it until $\tilde{f}(\vec{\epsilon})$ reaches one. This gives a plateau region $\epsilon^*(\epsilon_X, \epsilon_Y)$. Although the bounds found are not tight, they are strictly upper bounds of the associated LHS bounds. In the range $\epsilon_X, \epsilon_Y \in [0, 0.01]$ the estimated plateau length obtained via the formula (B2) at worst deviates from the values obtained by brute-force optimization by a factor $O(10^{-3})$. Considering that the plateau length is of the same order, $O(10^{-3})$, this deviation is quite significant. At best, the deviation is of the order $O(10^{-5})$.

2. Taylor expansion

Alternatively, the plateau region can be approximated using Taylor expansion. Associating each of Bob's lab measurement B_i with the Bloch vector $\vec{b}_i = (b_{ix}, b_{iy}, b_{iz})$, we observe that

$$f(\vec{\epsilon}) = \max_{\psi, B_y^{\epsilon_y}} \frac{1}{2} \langle B_1 + B_2 + B_3 \rangle_{\psi} = \max_{\psi, B_y^{\epsilon_y}} \frac{1}{2} \vec{\mathbf{b}} \times \vec{\psi} = \max_{B_y^{\epsilon_y}} \frac{1}{2} |\vec{\mathbf{b}}| \quad (\text{B3})$$

where $\vec{\mathbf{b}} = (\sum_i b_{ix}, \sum_i b_{iy}, \sum_i b_{iz})$. Moreover, Eq. (B3) is maximised when the deviation between the lab and the associated target measurement is taken to be as large as possible. Given this, the fidelity constraint then yields that the Bloch vectors $\vec{b}_i = (\sin \theta_i \cos \varphi_i, \sin \theta_i \sin \varphi_i, \cos \theta_i)$ optimally are chosen as

$$\begin{aligned} \vec{b}_x &= (a_x, \sqrt{\sin^2 \theta_x - a_x^2}, \cos \theta_x) \\ \vec{b}_y &= (\sqrt{\sin^2 \theta_y - a_y^2}, a_y, \cos \theta_y) \\ \vec{b}_z &= (\sqrt{1 - a_z^2} \cos \varphi_z, \sqrt{1 - a_z^2} \sin \varphi_z, a_z) \end{aligned}$$

where we have denoted $a_i = 1 - 2\epsilon_i$ for $i = x, y, z$. Moreover, we require that $\sin \theta_j \geq a_j$ for $j = x, y$. Next, inserting the the optimal \vec{b}_i into the Eq. (B3), we find that

$$f(\vec{\epsilon}) = \max_{\theta_x, \theta_y, \varphi_z} 2 \left((a_x + \sqrt{\sin^2 \theta_y - a_y^2} + \sqrt{1 - a_z^2} \cos \varphi_z)^2 + (\sqrt{\sin^2 \theta_x - a_x^2} + a_y + \sqrt{1 - a_z^2} \sin \varphi_z)^2 + (\cos \theta_x + \cos \theta_y + a_z)^2 \right)^{1/2}. \quad (\text{B4})$$

At this point, we want to compute the plateau region in terms of ϵ_Z for fixed pair of (ϵ_X, ϵ_Y) . Thus, solving $f(\vec{\epsilon}) = 1$ in terms of ϵ_Z yields

$$\epsilon_Z(\epsilon_X, \epsilon_Y) = \min_{\theta_x, \theta_y, \varphi_z} \frac{1}{2} \left(1 - \frac{d_2 + \sqrt{d_2^2 - d_1 d_3}}{2d_1} \right) \quad (\text{B5})$$

where we have denoted

$$\begin{aligned} d_1 &= (\cos \theta_x + \cos \theta_y)^2 + e_1^2 \\ d_2 &= (\cos \theta_x + \cos \theta_y) e_2 \\ d_3 &= e_2^2 - 4e_1^2 \\ e_1 &= a_x \cos \varphi_z + a_y \sin \varphi_z + \sqrt{\sin^2 \theta_y - a_y^2} \cos \varphi_z \\ &\quad + \sqrt{\sin^2 \theta_x - a_x^2} \sin \varphi_z \\ e_2 &= 1 - 2(a_x \sqrt{\sin^2 \theta_y - a_y^2} + a_y \sqrt{\sin^2 \theta_x - a_x^2} \\ &\quad + \cos \theta_x \cos \theta_y). \end{aligned} \quad (\text{B6})$$

Under the assumption that the measurement imprecisions are small, we can now employ Taylor expansion to approximate the trigonometric functions. In accordance with the target observables, we choose the expansion points to be $\theta_x : \pi/2, \theta_y : \pi/2$ and $\varphi_z : \pi/4$. From these, Taylor expansion up to first order gives that

$$\begin{aligned} \sin \theta_x &\approx 1 - \epsilon_X \\ \sin \theta_y &\approx 1 - \epsilon_Y \\ \sin \varphi_z &\approx \frac{1 + \sqrt{\epsilon_X/2} - \sqrt{\epsilon_Y/2}}{\sqrt{2}} = s_z \end{aligned} \quad (\text{B7})$$

Inserting the approximations (B7) back into the variables e_1 and e_2 we obtain that

$$\begin{aligned} e_1 &\approx (1 - 2\epsilon_X)c_z + (1 - 2\epsilon_Y)s_z + \sqrt{\epsilon_Y(2 - 3\epsilon_Y)}c_z \\ &\quad + \sqrt{\epsilon_X(2 - 3\epsilon_X)}s_z \\ e_2 &\approx 1 - 2((1 - 2\epsilon_X)\sqrt{\epsilon_Y(2 - 3\epsilon_Y)} \\ &\quad + (1 - 2\epsilon_Y)\sqrt{\epsilon_X(2 - 3\epsilon_X)} \\ &\quad + \sqrt{\epsilon_X(2 - \epsilon_X)}\sqrt{\epsilon_Y(2 - \epsilon_Y)}) \end{aligned} \quad (\text{B8})$$

where we have denoted $c_z = \sqrt{1 - s_z^2}$. We note that the final expressions only depends on the imprecision parameters ϵ_X and ϵ_Y . Thus, using Taylor expansion we eliminate the plateau length's dependence on the original optimization parameters $(\theta_x, \theta_y, \varphi_z)$. At worst, this methods gives that the values of the plateau lengths deviates from the numerical optimized bounds at an order of $O(10^{-4})$ for $\epsilon_X, \epsilon_Y \in [0, 0.01]$. However, for most input pairs (ϵ_X, ϵ_Y) the values only differ at an order of $O(10^{-5})$.

Appendix C: Semidefinite programming method

1. Bounding witnesses

We discuss an SDP relaxation method to bound arbitrary linear witnesses in an LHS model with imprecise measure-

ments. Define an operator list $L = \{\mathbb{1}, \sigma, \{B_{b|y}^{\text{targ}}\}, \{B_{b|y}^{\vec{\epsilon}}\}\}$. Over L , define an arbitrary monomial list, \mathcal{S} , with products of at least length one (i.e. the list L). Define the $|\mathcal{S}| \times |\mathcal{S}|$ moment matrix as

$$\Gamma_{u,v} = \text{tr}(u^\dagger v) \quad (\text{C1})$$

for $u, v \in \mathcal{S}$. By construction, we have $\Gamma \succeq 0$. In order to impose that all operators are d -dimensional, we use the sampling heuristic proposed in [28], and to impose the imprecision conditions (3) we use ideas of [10]. That is, we sample L randomly over \mathbb{C}^d , with the exception of $\{B_{b|y}^{\text{targ}}\}$. This procedure is repeated independently and the associated moment matrix samples are denoted $\{\Gamma^{(i)}\}_{i=1}^n$. The routine is terminated when the next sample is linearly dependent on the set of previously generated samples. The final moment matrix is then an affine combination over this basis,

$$\Gamma = \sum_{i=1}^n s_i \Gamma^{(i)} \quad \text{with} \quad \sum_i s_i = 1, \quad (\text{C2})$$

for some coefficients $\{s_i\}$. The imprecision conditions can then be imposed as linear inequalities, namely

$$\Gamma_{B_{b|y}^{\text{targ}}, B_{b|y}^{\vec{\epsilon}}} \geq 1 - \epsilon_{by}. \quad (\text{C3})$$

Over this domain, we optimise the witness value for LHS models with imprecise measurements. This is done independently for every deterministic strategy of Alice, characterised by the response functions $D_\lambda(a|x) \in \{0, 1\}$. Thus, we write

$$W_{\vec{\epsilon}}^\lambda = \sum_{a,b,x,y} c_{abxy} D_\lambda(a|x) \Gamma_{\sigma, B_{b|y}^{\vec{\epsilon}}}, \quad (\text{C4})$$

This constitutes an SDP. Solving the SDP for every deterministic strategy λ , we obtain an upper bound $W_{\vec{\epsilon}}^\lambda \leq \alpha^\lambda$. Our final bound on the witness is then obtained from

$$W_{\vec{\epsilon}} \leq \max_\lambda \{\alpha^\lambda\}. \quad (\text{C5})$$

In the main text, we discussed applying this method to bound the plateau length for the ESI witness when each of Bob's measurements has an independent imprecision parameter, $\vec{\epsilon} = (\epsilon_X, \epsilon_Y, \epsilon_Z)$. In Fig. 4, we illustrate the plateau length in ϵ_Z as a function of (ϵ_X, ϵ_Y) . All values match those obtained with seesaw search (interior point method) to five decimals. Therefore, this can for practical purposes be seen as a proof of the plateau length.

2. Imprecise LHS models for correlations

The SDP relaxations can be further extended to apply directly to probability distributions, $p_{\text{targ}}(a, b|x, y)$, without any reference to a specific witness. For this purpose, we associate a set of variables $\{s_i^\lambda\}_i$ to each deterministic strategy λ , and a corresponding moment matrix

$$\Gamma^\lambda = \sum_{i=1}^n s_i^\lambda \Gamma^{(i)} \quad \text{with} \quad \sum_{i,\lambda} s_i^\lambda = 1, \quad (\text{C6})$$

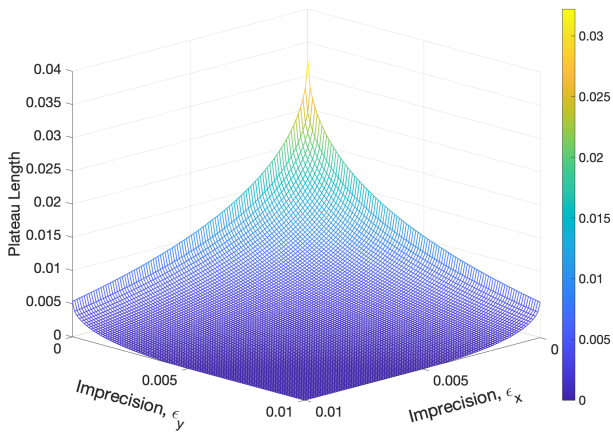


FIG. 4. Imprecision plateau for the ESI witness where each of the trusted parties measurements are associated with an independent imprecision parameter. The plateau length in ϵ_Z on the z-axis is given as a function of (ϵ_X, ϵ_Y) .

where $\Gamma^{(i)}$ still is the sampled moment matrix basis. We require that $\Gamma^\lambda \succeq 0$. The imprecision condition takes the form

$$\Gamma_{B_{b|y}, B_{b|y}}^\lambda \geq (1 - \epsilon_{by})q(\lambda), \quad (C7)$$

where $q(\lambda) = \sum_i s_i^\lambda$ is the probability of running strategy λ .

As a natural benchmark, we use an isotropic noise model, corresponding to the constraints $\forall a, b, x, y$,

$$vp_{\text{targ}}(a, b|x, y) + \frac{1-v}{N^2} = \sum_{a,b,x,y} \sum_{\lambda} c_{abxy} D_\lambda(a|x) \Gamma_{\sigma, B_{b|y}}^\lambda, \quad (C8)$$

where N is the number of outputs per party. Over this SDP domain, we optimise $v \in [0, 1]$. In order to prove that a given set of imprecision parameters $\vec{\epsilon}$ falls within a plateau, we must find that the solution of the SDP is identical to the critical visibility for standard steering with idealised measurements. The latter can be easily computed [2].

To test it, we have considered p_{targ} obtained from Alice and Bob sharing $|\phi^+\rangle$ and both measuring the three directions corresponding to an equilateral triangle in the XZ-plane of the Bloch sphere. The Bloch vectors are $(1, 0, 0)$, $(-\frac{1}{2}, 0, \frac{\sqrt{3}}{2})$ and $(-\frac{1}{2}, 0, -\frac{\sqrt{3}}{2})$ for both parties. When $\epsilon = 0$, these correlations have a steering visibility of $v = \frac{2}{3}$. Using the first level SDP relaxation, we find an imprecision plateau with length $\epsilon^* \approx 0.0287$. This is nearly an order of magnitude larger than the plateau obtained for the ESI witness, but notably its noise tolerance for detecting ρ_v is also significantly worse.

Appendix D: Detection efficiency for ESI witness and Pauli witness

Consider steering with imprecise measurements with lossy detection. Alice's measurements succeed only with probability η . With probability $1 - \eta$ she records a failed detection.

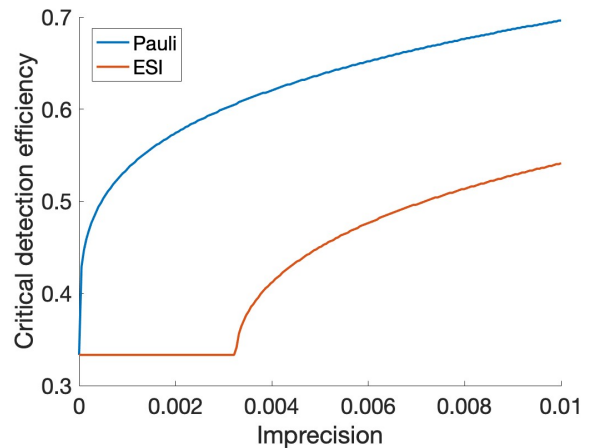


FIG. 5. We illustrate the critical detection efficiency η_{crit} for the Pauli and the ESI witness as a function of ϵ .

Our goal is select a quantum strategy that permits detection of steerability for the smallest possible η and realistic values of imprecision ϵ .

For the ESI witness, let the shared state be the partially entangled state $|\psi_\theta\rangle = \cos\theta|00\rangle + \sin\theta|11\rangle$. Moreover, select Alice's four measurements as corresponding to the Bloch vectors

$$\begin{aligned} \vec{a}_1 &= (t, t, 1)/\sqrt{t^2 + 1}, & \vec{a}_2 &= (t, -t, -1)/\sqrt{t^2 + 1}, \\ \vec{a}_3 &= (-t, t, -1)/\sqrt{t^2 + 1}, & \vec{a}_4 &= (-t, -t, 1)/\sqrt{t^2 + 1}, \end{aligned} \quad (D1)$$

where the parameter $t = \sin(2\theta)$. This gives the witness value

$$\mathcal{W}_0 = \sqrt{2 - \cos(4\theta)}. \quad (D2)$$

When her measurement fails, Alice outputs deterministically according to the strategy $\vec{a}_x = (a_1, a_2, a_3, a_4) \rightarrow (0, 1, 1, 0)$ which yields the witness value $C_\theta = 2\cos^2\theta - 1$. Solving the equation $\eta\mathcal{W}_0 + (1 - \eta)C_\theta = 1$, where we have the standard LHS bound on the right hand side, yields that the critical detection efficiency is given by

$$\eta_{\text{crit}} = \frac{2\sin^2\theta}{\sqrt{2 - \cos(4\theta)} - \cos(2\theta)} \quad (D3)$$

valid for $\theta \in [0, \frac{\pi}{4}]$. In the limit $\theta \rightarrow 0$, we obtain the optimal value $\eta_{\text{crit}} = 1/3$. In comparison, the same critical detection efficiency can be achieved with the Pauli steering witness. However, in the presence of imprecise measurements, the critical detection efficiency of the former stays constant within the plateau length whereas the latter rapidly deteriorates, see Figure 5.

Finally, the advantage owing to the plateau persists even when comparing ESI to steering inequalities with more settings, which for perfect measurements can arbitrarily reduce η_{crit} . For example, consider the ten-setting steering witness $\mathcal{W}_0 = \frac{1}{10} \sum_{x=1}^{10} \langle A_x B_x^{\text{targ}} \rangle$, where Bob's target measurements correspond to the vertices of the dodecahedron on the Bloch

sphere. It holds that $\mathcal{W}_0 \leq (3 + \sqrt{5})/10$ for LHS models [17] and $\eta_{\text{crit}} \approx 0.227$ [36]. While for perfect measurements this is significantly lower than the efficiency needed for the ESI, the situation is the opposite when operating at $\epsilon = \epsilon^*$: the LHS bound increases to $\mathcal{W}_{\epsilon^*} \lesssim 0.6081$ and the critical efficiency increases to $\eta_{\text{crit}} \approx 0.53$.

Appendix E: Beyond qubits

We now present a witness featuring an imprecision plateau tailored for four-dimensional quantum systems. The witness is inspired by Bell inequalities tailored for so-called random access codes [33]. Alice and Bob both have binary outcomes. Alice has eight inputs, which we write as a four-bit string where the first bit is fixed to zero, $x = 0x_2x_3x_4$, whereas $x_2, x_3, x_4 \in \{0, 1\}$. Bob has four inputs, $y = 1, 2, 3, 4$, which we associate with target observables $B_1^{\text{targ}} = X \otimes X$, $B_2^{\text{targ}} = Y \otimes X$, $B_3^{\text{targ}} = Z \otimes X$, $B_4^{\text{targ}} = \mathbb{1} \otimes Y$. By standard methods, one can verify that the LHS bound of following steering witness is eight

$$\mathcal{W}_0 \equiv \sum_{x_2, x_3, x_4, y} (-1)^{x_y} \langle A_x, B_y \rangle \stackrel{\text{LHS}}{\leq} 8. \quad (\text{E1})$$

Notably, by distributing a four-dimensional maximally entangled state and selecting suitable measurements for Alice, one can achieve the violation $\mathcal{W}_0 = 16$. It is also interesting to note that local hidden variable models cannot exceed $\mathcal{W} \leq 12$.

1. Imprecision plateau

We now aim to determine the LHS bound of Eq. (E1) under the assumption that all measurements are equally imprecise. We analyse the 256 deterministic strategies of Alice and find that they, up to symmetries, can be grouped in seven different classes

$$\begin{aligned} \mathcal{W}_\epsilon &= 8 \langle B_1 \rangle_\psi &&= g^*(\epsilon) \\ \mathcal{W}_\epsilon &= 2 \langle 3B_1 + B_2 + B_3 + B_4 \rangle_\psi \\ \mathcal{W}_\epsilon &= 4 \langle B_1 + B_2 + B_3 \rangle_\psi &&= f^*(\epsilon) \\ \mathcal{W}_\epsilon &= 4 \langle B_1 + B_2 \rangle_\psi \\ \mathcal{W}_\epsilon &= 2 \langle B_1 + B_2 + B_3 + B_4 \rangle_\psi \\ \mathcal{W}_\epsilon &= 4 \langle B_1 \rangle_\psi \\ \mathcal{W}_\epsilon &= 0 \end{aligned} \quad (\text{E2})$$

Three of these classes have no ϵ -dependence, in particular the first class $g(\epsilon) \equiv \max g^*(\epsilon) = 8$, which gives the standard LHS bound in (E1). The remaining four classes are ϵ -dependent. Of these, the strategy corresponding to $f^*(\epsilon)$ has the largest value. Therefore, to then compute the plateau length associated with the scenario, we want to evaluate $f(\epsilon) = \max f^*(\epsilon)$. Since we no longer can rely on Bloch sphere symmetries, we rely instead on our generalisation of the Lemma introduced in Ref. [15] so that it applies to target measurements of higher rank than one. This is discussed in

Appendix F. Here, we directly use the result, which is that for all

$$B_{b|y} \preceq (1 + \mu) B_{b|y}^{\text{targ}} + \frac{\sqrt{\mu^2 + 4(2\epsilon)(1 + \mu)} - \mu}{2} \mathbb{1}. \quad (\text{E3})$$

However, since Bob's target measurements are products of single-qubit observables, we consider the lab measurement to factor- by each single-qubit observable having an $\tilde{\epsilon}$ -imprecision (except the identity observable). This implies that $\epsilon = 2\tilde{\epsilon}$. Inserting (E3) into the expression for $f^*(\epsilon)$, we find that the expectation value over the target observables $B_y^{\text{targ}} \in \mathcal{H}_1 \otimes \mathcal{H}_2$ can be decomposed as follows

$$\langle B_1^{\text{targ}} + B_2^{\text{targ}} + B_3^{\text{targ}} \rangle_\psi = \text{Tr}((X + Y + Z) \text{Tr}_{\mathcal{H}_2}(\mathbb{1} \otimes X\psi)). \quad (\text{E4})$$

We recognize that ψ is optimally chosen such that partial trace over the second subsystem becomes

$$\text{Tr}_{\mathcal{H}_2}(\mathbb{1} \otimes X\psi) = \frac{\mathbb{1} + (1, 1, 1)/\sqrt{3} \times \vec{\sigma}}{2}. \quad (\text{E5})$$

At this point, the task to evaluate the upper bound of $f^*(\epsilon)$ is analogous to the procedure described in Appendix A. Following this, we find that

$$f(\epsilon) = \max_{\psi, B_y^{\epsilon_y}} f^*(\tilde{\epsilon}) \leq 4\sqrt{3} + 8\sqrt{6}\sqrt{2\epsilon(1-2\epsilon)} - 16\sqrt{3}\epsilon = \tilde{f}(\epsilon), \quad (\text{E6})$$

In fact, for every value of ϵ , we find that $\tilde{f}(\epsilon)$ match the value of $f(\epsilon)$. This can be verified by computing $\tilde{f}(\epsilon)$ through the see-saw method. This implies that $\tilde{f}(\epsilon)$ gives a tight bound. Lastly, solving $\tilde{f}(\epsilon) = 8$, we find that the threshold, at which the third class overtakes the first, is given by

$$\tilde{\epsilon}^* = \frac{9 - 2\sqrt{3} - \sqrt{3}}{32}. \quad (\text{E7})$$

Specifically, the threshold error of each qubit is then $\tilde{\epsilon}^* \approx 8.1 \times 10^{-4}$. This is large enough to encompass the imprecisions for X and Z Pauli operators experimentally observed in Ref. [18].

2. Detection efficiency for ququart entanglement

Consider the witness \mathcal{W}_0 in Eq. (E1) with lossy detection on Alice's side. Similarly to Appendix D, we want to compute the critical detection efficiency, η_{crit} , required for Bob to be able to detect steering within the plateau length. When Alice's detector fails she deterministically assign her output values in accordance with the first class of strategies in Eq. (E2). Additionally, we make the ansatz that the shared state between the parties is given by

$$|\Psi\rangle_{AB} = \frac{\cos \theta}{\sqrt{2}} |00\rangle + \frac{\sin \theta}{\sqrt{2}} |11\rangle + \frac{\sin \theta}{\sqrt{2}} |22\rangle + \frac{\cos \theta}{\sqrt{2}} |33\rangle, \quad (\text{E8})$$

valid for $\theta = [0, \pi/4]$. This yields that the value of the steering witness becomes $C_\theta = 8(2 \cos^2 \theta - 1)$. The eigenvalue

problem of finding the optimal quantum value Q_θ is then computed numerically. By solving $\eta Q_\theta + (1 - \eta)C_\theta = 8$ for fix θ , we obtain the optimal detection efficiency $\eta_{\text{crit}} = 1/4$ in the limit $\theta \rightarrow 0$.

In fact, the quantum value Q_θ obtained through the ansatz (E8) is optimal. This can be verified by alternatively calculating this value over an arbitrary steering assemblage $\{\sigma_{a|x}\}$ for fix η . We formulate this optimisation task as an SDP

$$\begin{aligned} \max_{\{\sigma_{a|x}\}} \quad & Q = \sum_{abxy} c_{abxy} \text{Tr}(B_{b|y}^{\text{targ}} \sigma_{a|x}) \\ \text{subject to} \quad & \eta Q + (1 - \eta)C = 8 \\ & \sigma_{a|x} \succeq 0 \quad \forall a, x \\ & \text{Tr}(\sum_a \sigma_{a|x}) = 1 \quad \forall x \\ & \sum_a \sigma_{a|x} = \sum_a \sigma_{a|x'} \quad \forall x, x' \end{aligned} \quad (\text{E9})$$

where we express the steering value as $C = 8 \text{Tr}(B_1^{\text{targ}} \sum_a \sigma_{a|x})$. The optimal quantum values Q_θ and Q are illustrated in Fig. 6 as a function of η_{crit} . The former is obtained from the ansatz (E8) (blue curve), whereas the latter is computed via (E9) (yellow curve).

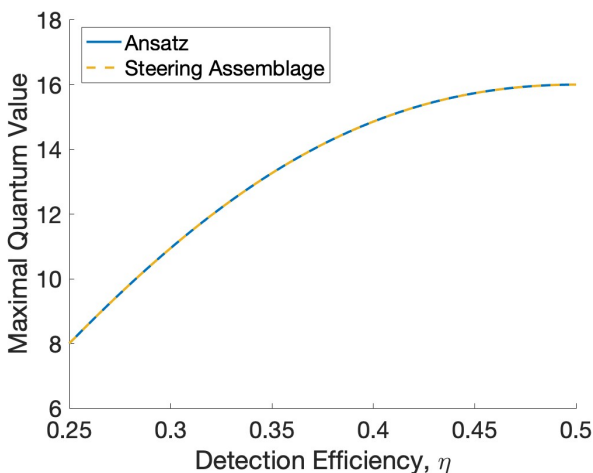


FIG. 6. We compare (Q_θ, η_θ) from ansatz (E8) (blue solid curve) with (Q, η) alternatively obtained via the SDP formulation in (E9) (yellow dashed curve).

Appendix F: Generalization of theorem of Ref. [15]

We generalize the main theorem introduced in Ref. [15] such that it applies to projective target measurements of rank greater than one when the trace of the lab measurement equals the rank of the target measurements.

Consider the the set of lab measurement $\{B_{b|y}\}$ in dimension D . The lab measurements are only constrained such that the fidelity of each POVM is limited by

$$\text{Tr}(B_{b|y} B_{b|y}^{\text{targ}}) \geq r(1 - \epsilon_{by}) \quad (\text{F1})$$

where $B_{b|y}^{\text{targ}} = \sum_{k=1}^r |\psi_k\rangle\langle\psi_k|$ is the projective target measurement of rank r and ϵ_{by} is the imprecision parameter associated to the y 'th measurement with outcome b . Next, we define the semidefinite operator

$$N = (1 + \mu_{by})B_{b|y}^{\text{targ}} + \eta_{by}\mathbb{1}_D \quad (\text{F2})$$

for some parameters $\mu_{by} \geq -1$ and $\eta_{by} \geq 0$. The goal is to find parameters (μ_{by}, η_{by}) such that $R \equiv \langle\chi|N - B_{b|y}|\chi\rangle \geq 0$ for every state $|\chi\rangle$ and measurement $B_{b|y}$ subject to (F1). Thus, we start by decomposing $B_{b|y}$ into the eigenbasis of the target measurement. This is done as follows: First, let $B_{b|y} = \sum_i q_i |\phi_i\rangle\langle\phi_i|$ for some pure states ϕ_i and set $\{q_i\}$ such that $\sum_i q_i = \text{Tr}(B_{b|y}) = r$, where $0 \leq q_i \leq 1$. Furthermore, each pure state in the ensemble can be decomposed into

$$|\phi_i\rangle = \sqrt{1 - \xi_i} |\tilde{\psi}_i\rangle + \sqrt{\xi_i} |\tilde{\psi}_i^\perp\rangle, \quad 0 \leq \xi_i \leq 1, \quad (\text{F3})$$

where $|\tilde{\psi}_i^\perp\rangle$ is some state orthogonal to $|\tilde{\psi}_i\rangle \in \mathcal{H}_{\text{targ}}$. Next, we express $|\tilde{\psi}_i\rangle$ in the eigenbasis of $B_{b|y}^{\text{targ}}$, i.e., $|\tilde{\psi}_i\rangle = \sum_{j=1}^r z_j^i |\psi_j\rangle$, where $\sum_j |z_j^i|^2 = 1$ to preserve normalization of the state. In particular, we let $z_j^i = e^{i\alpha_j^i} y_j^i$, where α_j^i is taken to be the relative phase between z_j^i and the first coordinate z_1^i , and y_j^i is the j 'th coordinate of the unit n -sphere ($n = r$). Explicitly, the coefficients are given by

$$\begin{aligned} z_1^i &= \cos \theta_1^i \\ z_j^i &= e^{i\alpha_j^i} \cos \theta_j^i \prod_{k=1}^{j-1} \sin \theta_k^i \quad j = 2, \dots, r-2 \\ z_{r-1}^i &= e^{i\alpha_{r-1}^i} \sin \varphi^i \prod_{k=1}^{r-2} \sin \theta_k^i \\ z_r^i &= e^{i\alpha_r^i} \cos \varphi^i \prod_{k=1}^{r-2} \sin \theta_k^i \end{aligned} \quad (\text{F4})$$

where the angles are defined for $\theta_j^i \in [0, \pi]$, $\varphi^i \in [0, 2\pi)$, and $\alpha_j^i \in [0, 2\pi)$. Note that $\alpha_1^i = 0$. We observe that the fidelity condition (F1) now can be written as

$$\sum_i q_i \xi_i \leq r \epsilon_{by}. \quad (\text{F5})$$

Now, to determine the parameters (μ_{by}, η_{by}) we expand R

$$R = \eta_{by} + (1 + \mu_{by}) \sum_{k=1}^r |\langle\chi|\psi_k\rangle|^2 - \sum_i q_i |\langle\chi|\phi_i\rangle|^2. \quad (\text{F6})$$

Specifically, the third term can be further expanded to

$$\begin{aligned} |\langle\chi|\phi_i\rangle|^2 &= (1 - \xi_i) \sum_j (y_j^i)^2 |\langle\chi|\psi_j\rangle|^2 \\ &\quad + \xi_i |\langle\chi|\tilde{\psi}_i^\perp\rangle|^2 \\ &\quad + 2(1 - \xi_i) \sum_{j < k} y_j^i y_k^i \text{Re}(e^{i(\alpha_j^i - \alpha_k^i)} \langle\chi|\psi_j\rangle \langle\psi_k|\chi\rangle) \\ &\quad + 2\sqrt{\xi_i(1 - \xi_i)} \sum_j y_j^i \text{Re}(e^{i\alpha_j^i} \langle\chi|\psi_j\rangle \langle\tilde{\psi}_i^\perp|\chi\rangle) \end{aligned} \quad (\text{F7})$$

At this point, we introduce the variables $x_j = \langle \chi | \psi_j \rangle = |x_j| e^{i\tilde{\phi}_j}$ and $x_i^\perp = \langle \chi | \psi_i^\perp \rangle = |x_i^\perp| e^{i\tilde{\phi}_i^\perp}$, where $\sqrt{\sum_j |x_j|^2 + |x_i^\perp|^2} \leq 1$, due to conservation of probability. Since we require that $R \geq 0$ for every choice of $(x_1, \dots, x_r, x_i^\perp)$ we can choose the phases such that $|\langle \chi | \phi_i \rangle|^2$ is maximised. This implies that $\tilde{\phi}_1 = \dots = \tilde{\phi}_r = \tilde{\phi}_i^\perp$ and that the relative phase $\alpha_j^i = 0$ for all j . Thus, we can without loss of generality proceed with $(x_1, \dots, x_r, x_i^\perp)$ being real parameters with the same sign, meaning that we constrain the angles to $\theta_j^i \in [0, \pi/2]$ and $\varphi^i \in [0, \pi/2]$. As a result,

$$|\langle \chi | \phi_i \rangle|^2 \leq \sum_i q_i (\sqrt{1 - \xi_i} \sum_j y_j x_j + \sqrt{\xi_i} x_i^\perp)^2 \quad (\text{F8})$$

From Cauchy-Schwartz inequality we now get that $\sum_j y_j x_j = \vec{y} \times \vec{x} \leq \|\vec{y}\| \|\vec{x}\| = \|\vec{x}\|$, since $\|\vec{y}\| = 1$. Denoting $x = \|\vec{x}\| = \sqrt{\sum_j x_j^2}$ and observing that R is minimised for $x_i^\perp = \sqrt{1 - x^2}$, we obtain

$$R \geq \eta_{by} - \sum_i q_i \xi_i + x^2 \left(\mu_{by} + 2 \sum_i q_i \xi_i \right) - 2x \sqrt{1 - x^2} \sum_i q_i \sqrt{\xi_i (1 - \xi_i)} \quad (\text{F9})$$

Thereafter, the rest of the argument follows directly from Ref. [15], which gives

$$\begin{aligned} B_{b|y} &\leq (1 + \mu_{by}) B_{b|y}^{\text{targ}} \\ &+ \frac{1}{2} \left(\sqrt{\mu_{by}^2 + 4(r\epsilon_{by})(1 + \mu_{by})} - \mu_{by} \right) \mathbb{1}_D \quad (\text{F10}) \\ &= (1 + \mu_{by}) B_{b|y}^{\text{targ}} + \frac{1}{2} z_{by}. \end{aligned}$$

Furthermore, z_{by} is non-negative and monotonically decreasing in μ_{by} . In this case, the $\bar{\epsilon}$ -dependent LHS bound of an arbitrary witness (1) is bounded by

$$\mathcal{W}_{\bar{\epsilon}} \leq \min_{\mu \geq -1} (1 + \mu) \beta_0 + \frac{1}{2} \sum_x \max_a \left(\sum_{by} c_{abxy} \tilde{z}_{by} \right) \quad (\text{F11})$$

where β_0 is the standard LHS bound for perfect measurements and parameters μ is optimally chosen such that the right-hand side of Eq. (F11) is minimised. This means that $\mu = \max_{by} \mu_{by}$, which gives

$$\tilde{z}_{by} = \sqrt{\mu^2 + 4(r\epsilon_{by})(1 + \mu)} - \mu. \quad (\text{F12})$$

Note that the result (F11) is general and that every choice of the parameter μ_{by} corresponds to a valid analytical bound.